NUMERICAL STUDY OF INDOOR POLLUTANT TRANSPORT FOCUSED ON THE GRADIENT-DIFFUSION HYPOTHESIS

Twan van Hooff[1,2], Bert Blocken[1], Pierre Gousseau[1] and GertJan van Heijst[3]
[1]Building Physics and Services, Eindhoven University of Technology, Eindhoven, the Netherlands
[2]Building Physics Section, Katholieke Universiteit Leuven, Leuven, Belgium
[3]Fluid Dynamics Laboratory, Eindhoven University of Technology, Eindhoven, the Netherlands.

ABSTRACT

The majority of numerical studies of room airflow using Computational Fluid Dynamics (CFD) are conducted with the steady Reynolds-averaged Navier-Stokes (RANS) approach. In this approach the averaged quantities are computed, and the effect of turbulence is modelled. Furthermore, the standard-gradient diffusion hypothesis is often used to model the turbulent mass transport, which relates the turbulent mass flux to the mean concentration derivative. In this paper, a CFD analysis of pollutant dispersion in an enclosure ventilated by a transitional wall jet (Re ≈ 2,500) is presented, using validated high-resolution RANS and Large Eddy Simulations (LES). Although the LES computations show that a counter-gradient turbulent mass flux is present, indicating that the standard gradient-diffusion hypothesis used in RANS is not valid in the entire flow domain, it is shown that the convective mass fluxes dominate over the turbulent mass fluxes, and that therefore the pollutant concentrations predicted by RANS do not differ significantly.

INTRODUCTION

Steady RANS simulations of dispersion generally use the standard gradient-diffusion (GD) hypothesis (the adjective "standard" will be omitted in the remainder of the paper). The GD hypothesis relates the turbulent mass flux to the mean mass concentration gradient using the turbulent (or eddy) mass diffusivity D_t. The value of D_t is deduced from the computed turbulent viscosity ν_t and the input value of the turbulent Schmidt number Sc_t ($D_t = \nu_t/Sc_t$). In general, a value for Sc_t between 0.5 and 0.9 is used. In the commercial CFD code Fluent 6.3 for example, the default value is 0.7 (Fluent 2006).

Although several publications focused on the value of Sc_t in the past, to the best knowledge of the authors, no earlier room airflow studies have been published in which the validity of the GD hypothesis is investigated. In other research areas, studies on this topic are very scarce as well. Tominaga and Stathopoulos (2007) provided some information about convective and diffusive fluxes for the case of dispersion around a building in an atmospheric boundary layer flow. Gousseau et al. (2011, 2012) published two articles in which they studied the validity of the GD hypothesis for pollutant dispersion around isolated buildings. For this study they compared high-resolution LES results with RANS results and found that a counter-gradient mechanism governs turbulent pollutant transfer in the streamwise direction.

In this paper, a detailed analysis of the transport process of a passive gaseous pollutant in a room ventilated by a transitional plane wall jet is presented. A transitional wall jet can be distinguished from a turbulent wall jet by the presence of large coherent structures in the wall jet region. First, the room geometry is described after which the experimental setup that has been used to obtain validation data for the numerical simulations will be presented. After that, the governing equations are addressed and the CFD model is described. Subsequently, the validation study is outlined, followed by the results of the pollutant dispersion simulations. Finally, a discussion and conclusions conclude the paper.

ROOM GEOMETRY

The room geometry under study is a cubical enclosure (L^3) with edges L = 0.3 m. A linear ventilation inlet is present at the top of the room with an inlet height of h/L = 0.1 and a width of w/L = 1. In addition, a linear ventilation outlet is present at the bottom of the opposite wall, with a height of h/L = 0.0167 (Fig. 1a). The chosen configuration represents a mixing ventilation case; the ventilation air enters the enclosure through the inlet in the upper part of the room (wall jet), it mixes with the room air, and the diluted air is exhausted through the outlet (e.g. Awbi 2003). This geometrical configuration is one of the most often studied configurations in ventilation research, and was used, among others, in the pioneering studies by Nielsen (1974) and Chen (1995, 1996).

An important dimensionless number for indoor airflow studies is the slot Reynolds number, which is defined based on the inlet height as $Re = U_0 h/\nu$, with U_0 the bulk inlet velocity and ν the kinematic viscosity at room temperature (≈ 20°C) (see Fig. 1b). A Re-value of 2,500 was used in this study, which was shown to result in transitional jet flow, including Kelvin-Helmholtz-type instabilities in the outer region (shear layer) of the wall jet (van Hooff et al. 2012a).

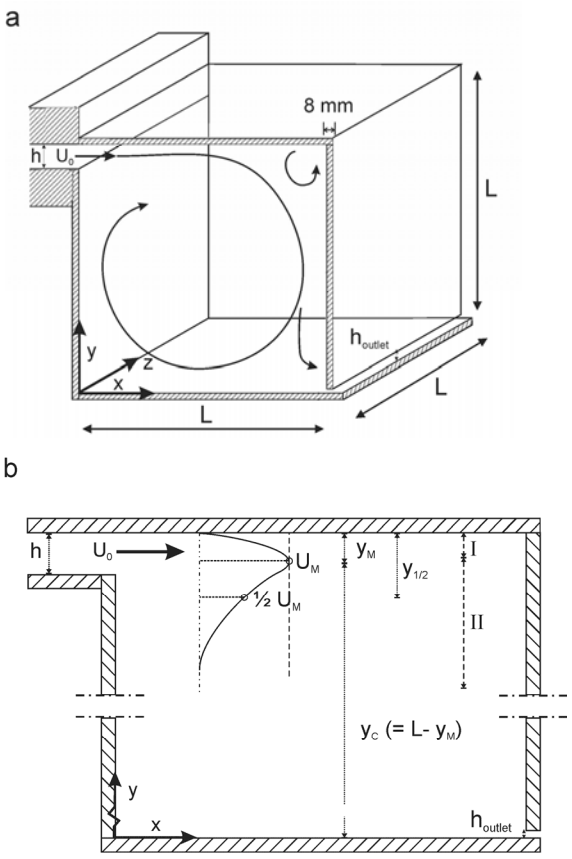

Fig. 1: (a) 3D room geometry with indication of the coordinate system, the inlet velocity U_0, the inlet height h, the outlet height h_{outlet} and the dimensions of the test section L^3. (b) 2D schematic representation of the plane wall jet with I the inner region, II the outer region, U_M the maximum velocity, y_M the distance from the top wall to the location of U_M, y_C the distance from the bottom wall to the location of U_M and $y_{1/2}$ the location of ½U_M in the outer region.

MODEL EXPERIMENTS

A water-filled model was used to perform Particle Image Velocimetry (PIV) measurements of the flow pattern in the test section for validation purposes (van Hooff et al. 2012a, 2012b). The reduced-scale model consists of a water column, a conditioning section and a cubic test section of 0.3 x 0.3 x 0.3 m^3 (Fig. 2a). More information on the experimental setup can be found in van Hooff et al. (2012b).

A 2D PIV system was used to conduct the measurements. It consisted of a Nd:Yag (532 nm) double-cavity laser (2 x 200 mJ, repetition rate < 10 Hz) used to illuminate the field of view, and one CCD (Charge Coupled Device) camera (1376 x 1040 pixel resolution, 10 frames/s) for image acquisition. The laser was mounted on a translation stage and was positioned above the cubic test section to create a laser sheet in the vertical centre plane of the cube (z/L = 0.5); the camera was positioned perpendicular to the laser sheet. Seeding of the water was provided by hollow glass micro spheres (3M; type K1) with diameters in the range of 30 – 115 µm.

Two sets of PIV measurements were performed. The first set focused on the entire cross-section of the cube, i.e. a target area of 0.3 x 0.3 m^2 (= ROI1) (Fig. 2b). The second set focused on a smaller target area of 0.18 x 0.12 m^2 (W x H) in the proximity of the inlet, enabling a higher measurement resolution (= ROI2) (see Fig. 2b). The uncertainty of the measurement results is around 2-4% in the largest part of the test section and is slightly higher than 4% in the shear layer and boundary layer areas as a result of the locally higher turbulence levels. Note that the results for y/L < 0.05 are not used because they are less accurate due to reflections of the laser sheet on the glass bottom of the cube. Additional measurement results for this specific room geometry with h/L = 0.1 and Re ≈ 2,500 can be found in van Hooff et al. (2012a). The measurement results will be presented later in this paper together with the results of the CFD simulations.

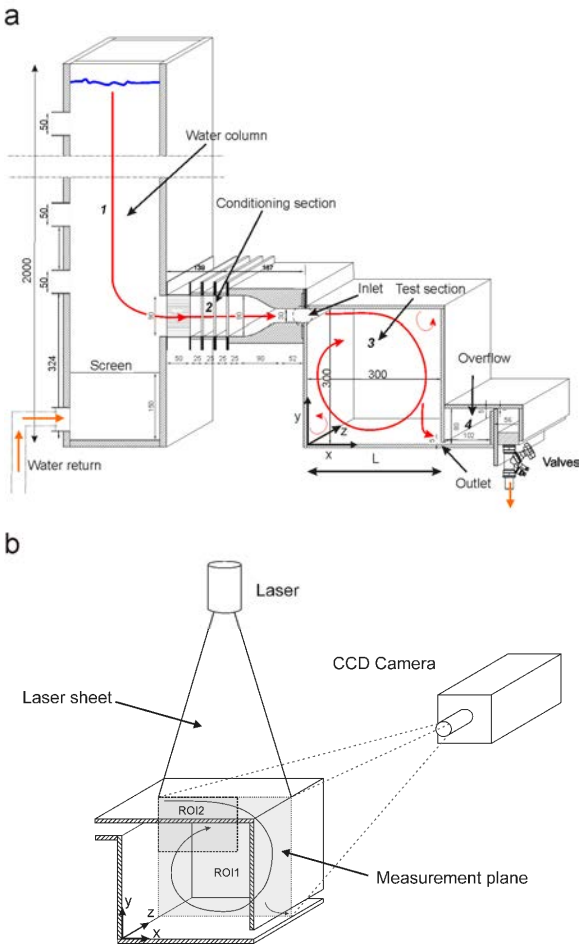

Fig. 2: (a) Reduced-scale setup used for the flow visualizations and PIV measurements. Dimensions in mm. (b) PIV measurement setup: ROI1 indicates the region of interest (L x L) for the first measurement set, ROI2 indicates the region of interest of 0.6L x 0.4L (W x H) for the second set.

RANS, LES AND DISPERSION MODELLING

RANS and turbulence models

In the RANS approach, the Reynolds decomposition splits the flow variables into an average and a fluctuating part. Only the averaged quantities are resolved and the effect of turbulence on the average flow field (Reynolds stresses) is modelled with turbulence models. In this study the Low Reynolds (LR) number k-ε model by Chang et al. (1995) is used for the RANS simulations.

LES and subgrid-scale models

In LES, a spatial-filtering operator is applied to the Navier-Stokes equations, which separates the large scales of motion from the small scales. The large scales of motion are explicitly resolved, and the small scales, which have a more universal behaviour, are modelled with a subgrid-scale (SGS) model. For the LES simulations in this paper, the dynamic Smagorinsky SGS model is used (Smagorinsky 1963, Germano et al. 1991, Lilly 1992). The application of LES has been especially interesting in studies of mass transport, since this process is mainly governed by the largest scales of motion.

Dispersion modelling

The instantaneous pollutant concentration c (kg m^{-3}) is treated as a scalar transported by an advection-diffusion equation (Eulerian approach):

$$\frac{\partial c}{\partial t} + \vec{u}.\nabla c = -\nabla.\overrightarrow{q_m} + s_c \qquad (1)$$

where $\vec{u}$ is the velocity vector, s_c a source term and $\overrightarrow{q_m}$ the mass flux due to molecular diffusion. Applying the Reynolds decomposition to the variables (x = X + x' where X = <x> and x' are the mean and fluctuating components of x, respectively) and averaging Eq. (1) yields:

$$\nabla.\left(\overrightarrow{Q_m} + \overrightarrow{Q_c} + \overrightarrow{Q_t}\right) = S_c \qquad (2)$$

In this equation, $\overrightarrow{Q_m}$ is the mean molecular mass flux (kg $m^{-2}s^{-1}$), which is proportional to the gradient of mean concentration:

$$Q_{m,i} = -D_m \frac{\partial C}{\partial x_i} \qquad (3)$$

where D_m is the molecular mass diffusivity (m^2 s^{-1}). In general, the molecular mass flux is negligible in comparison with the mean convective and turbulent fluxes, symbolized by $\overrightarrow{Q_c}$ and $\overrightarrow{Q_t}$, respectively. Note that the adjective "mean" will be omitted in the remainder of the paper. The convective mass flux is given by:

$$Q_{c,i} = U_i C \qquad (4)$$

And the turbulent mass flux is given by:

$$Q_{t,i} = < u_i' c' > \qquad (5)$$

However, the steady RANS models do not provide the velocity and concentration fluctuations. Therefore, the turbulent mass flux must be linked to the mean variables. In general, the GD hypothesis is adopted, by analogy with molecular diffusion:

$$Q_{t,i:RANS} = -D_t \frac{\partial C}{\partial x_i} \qquad (6)$$

where D_t is the turbulent mass diffusivity. The value of D_t is generally deduced from the computed turbulent viscosity ν_t and the input value of the turbulent Schmidt number $Sc_t = \nu_t/D_t$.

In LES, the total turbulent mass flux Q_t is the sum of the flux due to the resolved turbulent fluctuations and the mean SGS mass flux:

$$Q_{t,i;\ LES} = < \overline{u}_i' \overline{c}' > + < q_{SGS,i} > \qquad (7)$$

The instantaneous SGS mass flux $\overrightarrow{q_{SGS}}$ is assumed proportional to gradient of resolved concentration:

$$q_{SGS,i} = \overline{u_i c} - \overline{u}_i \overline{c} = -D_{SGS} \frac{\partial \overline{c}}{\partial x_i} \qquad (8)$$

where the overbar denotes the filtering operation and D_{SGS} is the SGS mass diffusivity. In this study, D_{SGS} is computed via the SGS viscosity ν_{SGS} and the SGS Schmidt number $Sc_{SGS} = \nu_{SGS}/D_{SGS}$. Here, Sc_{SGS} is computed dynamically, with a similar procedure as the Smagorinsky coefficient C_s (Moin et al. 1991). In the remainder of the paper all mean concentrations will be expressed in non-dimensional form as a concentration coefficient K:

$$K = \frac{C}{C_{ref}} \qquad (9)$$

where the reference concentration C_{ref} is defined as:

$$C_{ref} = \frac{S_c V}{h_{inlet}{}^2 U_0} \qquad (10)$$

with S_c the pollutant source rate (kg $m^{-3}s^{-1}$), V the enclosure volume (m^3), h_{inlet} the inlet height (m) and U_0 the inlet velocity (m s^{-1}). In addition, a reference flux magnitude Q_0 (kg $m^{-2}s^{-1}$) will be used to make the convective and turbulent mass fluxes non-dimensional. The reference flux magnitude Q_0 can be calculated from the inlet velocity and from the reference concentration C_{ref} (kg m^{-3}) as $Q_0 = C_{ref}U_0$.

CFD SIMULATIONS: SETTINGS AND PARAMETERS

Computational geometry and grid

The computational model is based on the experimental setup as described above and as previously presented in van Hooff et al. (2012c). Note that, since the simulations are also performed for the reduced-scale model, the simulations are also conducted with water as fluid (ρ = 998.2 kg m^{-3}). From the conditioning section, i.e. the contraction upstream of the test section, only a small part is included in the model (Fig. 3a). Please note that the outlet is extended in the x-direction to enhance convergence of the simulations.

The computational grid was created using the surface-grid extrusion technique presented in van Hooff and Blocken (2010). Both the steady RANS simulation and the LES simulation were conducted on a grid with 1,386,400 cells. The grid size was based on a grid-sensitivity analysis, which indicated nearly grid-independent results on the grid used in this paper (van Hooff et al. 2012c). The number of cells over the inlet height and outlet height is 50 and 20, respectively. The dimensionless wall distances y^* at the top surface (y/L = 1) in the centre plane (z/L = 0.5) are between 0.12 and 0.68. The low values for y^* enable the use of low-Reynolds number modelling (LRNM) for the RANS models, which implies solving the flow all the way down to the wall, including the thin viscous sublayer. The grid requirements for the application of LRNM are high: the cells should be small enough to result in y^* values which are preferably lower than 1. The numerical accuracy using LRNM is larger than when using wall functions, in which a semi-empirical formula is used to bridge the region from the wall to the centre of the wall-adjacent cell. Also for LES the y^* value should preferably be about 1 or smaller.

Boundary conditions

To replicate the PIV measurements as much as possible, the boundary conditions for the CFD simulations were chosen as close to those of the PIV experiments as possible. A uniform velocity was imposed at the CFD inlet (see Fig. 3a), the value of which was based on the Reynolds number at the actual ventilation inlet during the experiments and the ratio between the height of the CFD inlet (h/L = 0.3) and the actual ventilation inlet (h/L = 0.1); $U_{inlet;CFD}$ = 0.025 m s^{-1} for Re ≈ 2,500. Due to the contraction the velocity at the actual ventilation inlet is approximately three times higher than the one imposed at the CFD inlet. The turbulence parameters were specified based on the hydraulic diameter and the turbulence intensity. The hydraulic diameter D_h was calculated using $D_h = (4WH)/(2(W+H))$, with H the height and W the width of the CFD inlet. The measured turbulence intensity (u_{RMS}/U_M) in the wall jet region at x/L = 0.2 was around 3-4% (van Hooff et al. 2012a). U_M is the maximum local velocity and it will also be used in the remainder of the study to make the velocities non-dimensional (U/U_M) (Fig. 1b). Note that U_M is defined as the local maximum time-averaged x-velocity, and thus varies with both x/L and Re. A constant turbulence intensity of 18% was imposed at the CFD inlet. Due to the contraction the resulting turbulent kinetic energy values at the entrance of the cubic test section correspond with the measured values (see van Hooff et al. 2012c). For the LES computations, a time-dependent inlet profile is generated by using the vortex method (Sergent 2002) with a number of vortices N_v = 190. As shown by Sergent (2002), this parameter has only little influence on the generated velocity fluctuations. Zero static pressure was imposed at the outlet and the surfaces were modelled as smooth no-slip walls.

To incorporate pollutants, a constant and uniform pollutant source term S_c = 0.02 kg $m^{-3}s^{-1}$ was imposed in the whole cubic enclosure. The pollutant is passive and has the same density as the ambient fluid (= water: 998.2 kg m^{-3}), implying absence of buoyancy effects. The concentration at the ventilation inlet equals zero, which corresponds to the supply of fresh water.

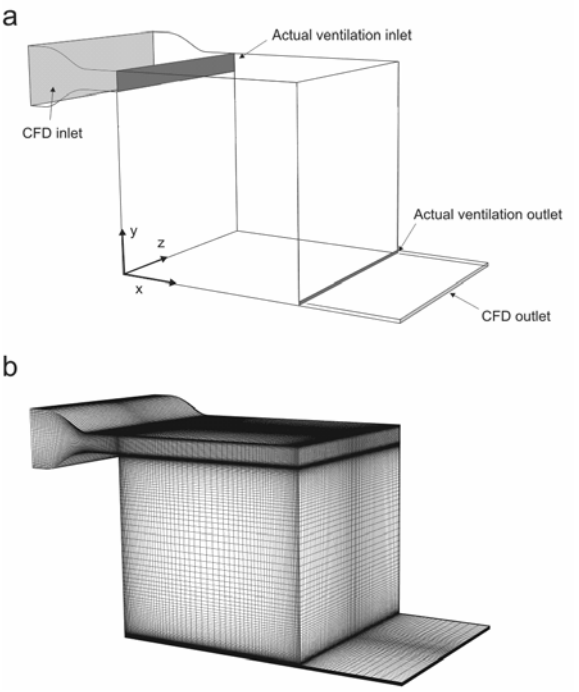

Fig. 3: (a) Computational model of the water cube. (b) Computational grid (1,386,400 cells).

Solver settings

For the RANS simulations, pressure-velocity coupling is taken care of by the SIMPLEC algorithm, pressure interpolation is second order and second-order upwind discretization schemes are used for all transport equations (momentum, turbulence and concentration). Convergence has been monitored

carefully. The dispersion simulation using RANS was conducted in two steps. First, the steady flow field was obtained. Second, the transport equation for concentration is solved to obtain the spatial distribution of the pollutant.

For the LES simulation, the filtered momentum equation is discretised with a bounded central-differencing scheme. A second-order upwind scheme is used for the concentration equation. Pressure interpolation is second order. Time integration is second-order implicit. Pressure-velocity coupling is taken care of by the PISO algorithm. The results of the LES computation presented here are averaged over 200,000 time steps, which corresponds to 800 s, which is 20 times the approximated value of t^*, which is the time needed for the jet to make one circulation in the test section, and which can be defined as $t^* = (4L)/U_{average}$, with $U_{average}$ the average velocity of the jet around the recirculation cell. The time step Δt was based on a maximum CFL number of 1 and is equal to $\Delta t = 0.004$ s. It was verified that the averaging time is sufficient to obtain statistically-steady results by monitoring the evolution of K with time (moving average) at several points inside the domain.

CFD SIMULATIONS: RESULTS

Mean velocities

Figure 4 compares the measured and simulated profiles of the time-averaged dimensionless x-velocity (U/U_M) along two vertical lines in the test section centre plane, at $x/L = 0.2$ and $x/L = 0.5$. From Figure 4 it can be concluded that the velocity profiles obtained with the LR k-ε model are in relatively close agreement with the measurements. Furthermore, Figure 4 shows that the profiles obtained with LES fit the PIV measurement results very well, the model does not perform significantly better than the LR k-ε model. In general, a good to very good agreement is obtained from both the steady RANS and the LES simulation.

Pollutant dispersion

In order to assess the accuracy of the LES simulations, the ratio of the magnitudes of subgrid-scale fluxes to turbulent fluxes ($\left|\overrightarrow{Q_{SGS}}/\overrightarrow{Q_t}\right|$) in the vertical centre plane ($z/L = 0.5$) has been calculated, in which $\langle q_{SGS,i}\rangle = Q_{SGS,i}$ in Eq. (7). This ratio appeared to be between 1.0E-02 and 1.0E-03 in the largest part of the flow domain, which indicates that the magnitude of the subgrid-scale fluxes is small compared to the turbulent fluxes. In general, this shows that with the currently applied grid resolution and SGS modelling the magnitude of the subgrid-scale fluxes is several orders of magnitude smaller than that of the turbulent fluxes. Please note that in accordance to Eq. (7) the SGS contribution is included in the definition of the turbulent mass flux in this and in consecutive figures. Figure 5 shows the non-dimensional convective mass fluxes ($Q_{c,i}/Q_0$) in the streamwise (Fig. 5a,c) and the vertical direction (Fig. 5b,d) obtained from the steady RANS simulation and the LES simulation (time-averaged). It can be seen that the contours obtained with steady RANS are quite similar compared to those from the unsteady LES simulation, both in shape and in the values of the non-dimensional convective fluxes. Only small differences in the shape of the contours are visible. The isolines for K = 0.04; 0.12; 0.20; 0.28 and 0.34 are plotted in Figure 5 as well.

The non-dimensional turbulent mass fluxes ($Q_{t,i}/Q_0$) are depicted in Figure 6. The turbulent mass fluxes from the LES simulation are calculated using Eq. (7). For the steady RANS simulation the turbulent fluxes are obtained using the GD hypothesis (Eq. (6)). The first observation that can be made is that the turbulent fluxes (Fig. 6) are considerably smaller than the convective fluxes in a large part of the domain, as depicted in Figure 5. In general, the absolute values of the turbulent fluxes $|Q_{t,i}/Q_0|$ are one order of magnitude smaller than the absolute values of the convective fluxes. The circles with a '+' or '-' sign indicate whether there is a positive or negative concentration derivative in the corresponding direction, respectively. Figure 6a,b shows the turbulent fluxes obtained from the RANS simulations. According to the GD hypothesis, the turbulent fluxes are positive in regions with negative concentration derivatives ($\partial C/\partial x < 0$; $\partial C/\partial y < 0$).

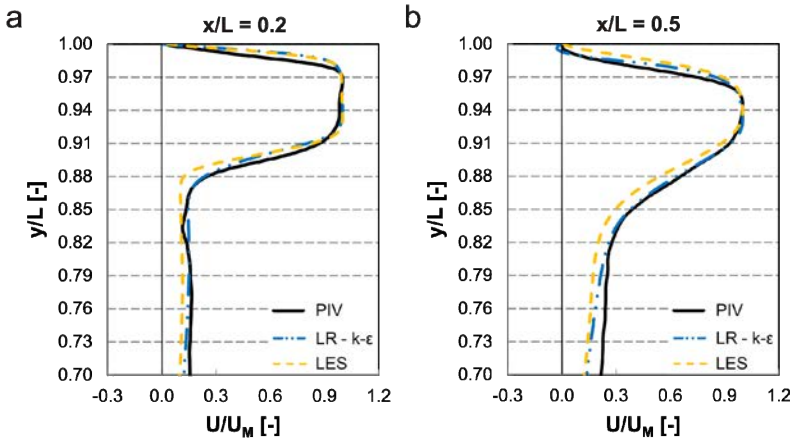

Fig. 4: Comparison of mean velocity profiles by PIV in ROI2 with results of steady RANS CFD simulations and LES simulation for Re ≈ 2,500. (a) U/U_M at x/L = 0.2; (b) U/U_M at x/L = 0.5.

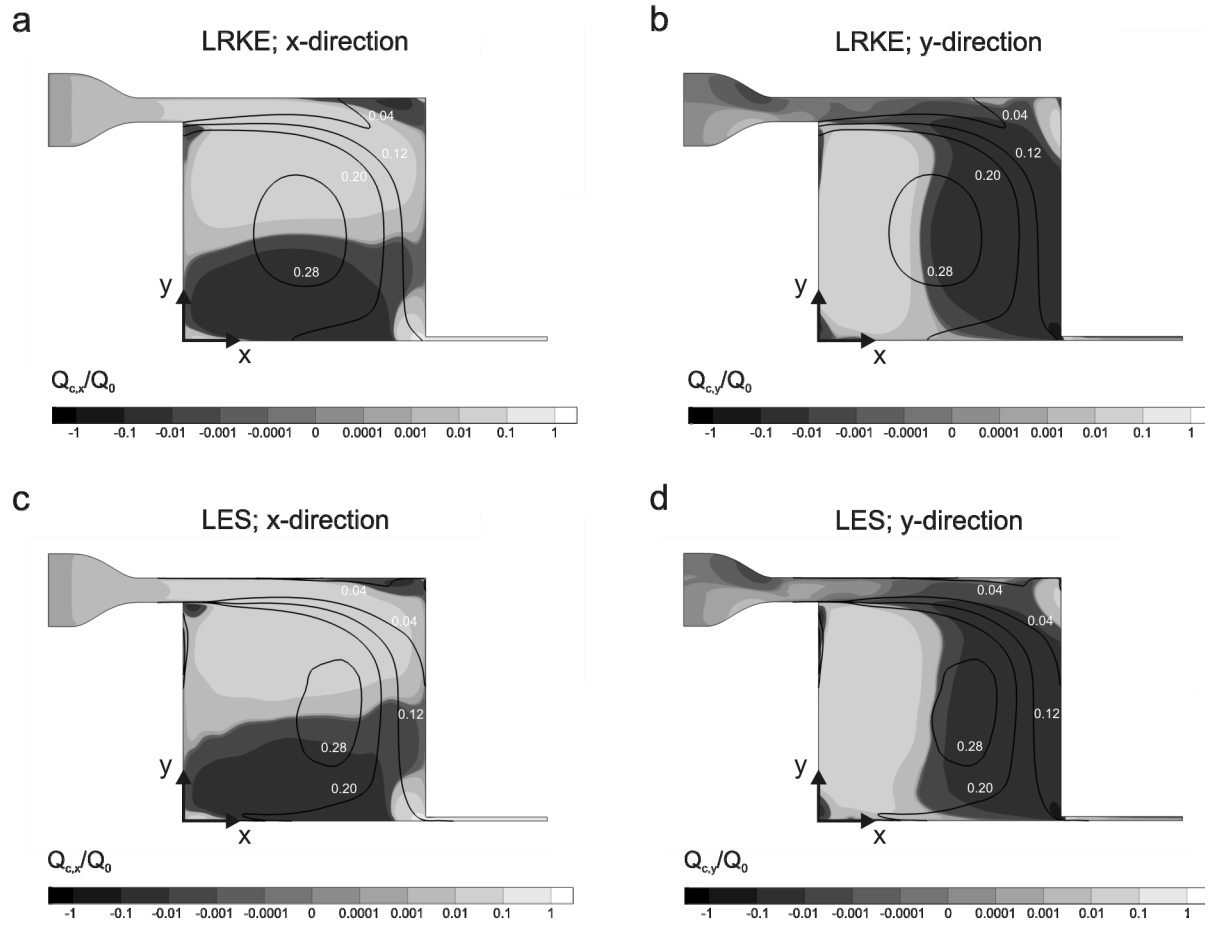

Fig. 5: Contours of the streamwise ($Q_{c,x}/Q_0$) (a,c) and vertical ($Q_{c,y}/Q_0$) (b,d) non-dimensional convective mass fluxes in the vertical centre plane (z/L = 0.5) of the enclosure obtained with steady RANS and LES. (a,b) Low-Reynolds k-ε (RANS). (c,d) LES. The solid lines are isolines of K = 0.04; 0.12, 0.20, 0.28 and 0.34.

Figure 6c,d shows the turbulent fluxes in the vertical centre plane obtained from the LES simulation. In addition to contours of $Q_{t,i}/Q_0$, the isoline $\partial C/\partial x = 0$ is depicted, as well as the areas with positive or negative concentration derivatives, indicated with a '+' or '-' sign, respectively. The contours of $Q_{t,i}/Q_0$ differ significantly from those obtained from the RANS simulations. Figure 6c shows that in the outer region of the wall jet there is a negative concentration gradient ($\partial C/\partial x < 0$) in the x-direction, while there is also a negative turbulent flux ($Q_{t,x}/Q_0 < 0$) in this region. This observation shows that the GD hypothesis is not valid in this region; a counter-gradient mass transport mechanism is present characterised by $Q_{t,i}$ and $\partial C/\partial x_i$ being of the same sign. The same holds for the region near the bottom surface and close to the wall containing the inlet; in this area a positive value of ($\partial C/\partial x > 0$) exists in combination with a positive turbulent mass flux ($Q_{t,x}/Q_0 > 0$). Figure 6d shows the turbulent fluxes in the vertical direction obtained with LES. It is shown that there is a region with $\partial C/\partial y < 0$ below the wall jet in combination with a negative turbulent mass flux ($Q_{t,y}/Q_0 < 0$). In the vicinity of the outlet a positive turbulent mass flux ($Q_{t,y}/Q_0 > 0$) is present in an area with $\partial C/\partial y > 0$. These observations indicate the fact that the GD hypothesis is not valid in the entire flow domain. The inability of the GD hypothesis to accurately predict the turbulent fluxes can be attributed to the effects of coherent structures inside the flow domain, which was also indicated by Gousseau et al. (2012) for dispersion around an isolated building. These coherent structures drive the counter-gradient transport in the enclosure. Figure 7 depicts vertical profiles of the calculated dimensionless concentrations K in the vertical centre plane of the enclosure obtained with RANS (LR k-ε in combination with the default value of $Sc_t = 0.7$) and LES. It can be seen that the results obtained with LES show a close agreement (within 10%) with the results obtained with the LR k-ε model. This observation can be made at all three locations and indicates that the use of the standard GD hypothesis does not lead to large discrepancies in the calculated pollutant concentration distribution, at least for this particular case. This can be attributed to the fact that the convective fluxes dominate over the turbulent fluxes; deviations in the turbulent fluxes therefore have only a relatively small influence on the total mass flux, and thus on the predicted pollutant concentration distribution.

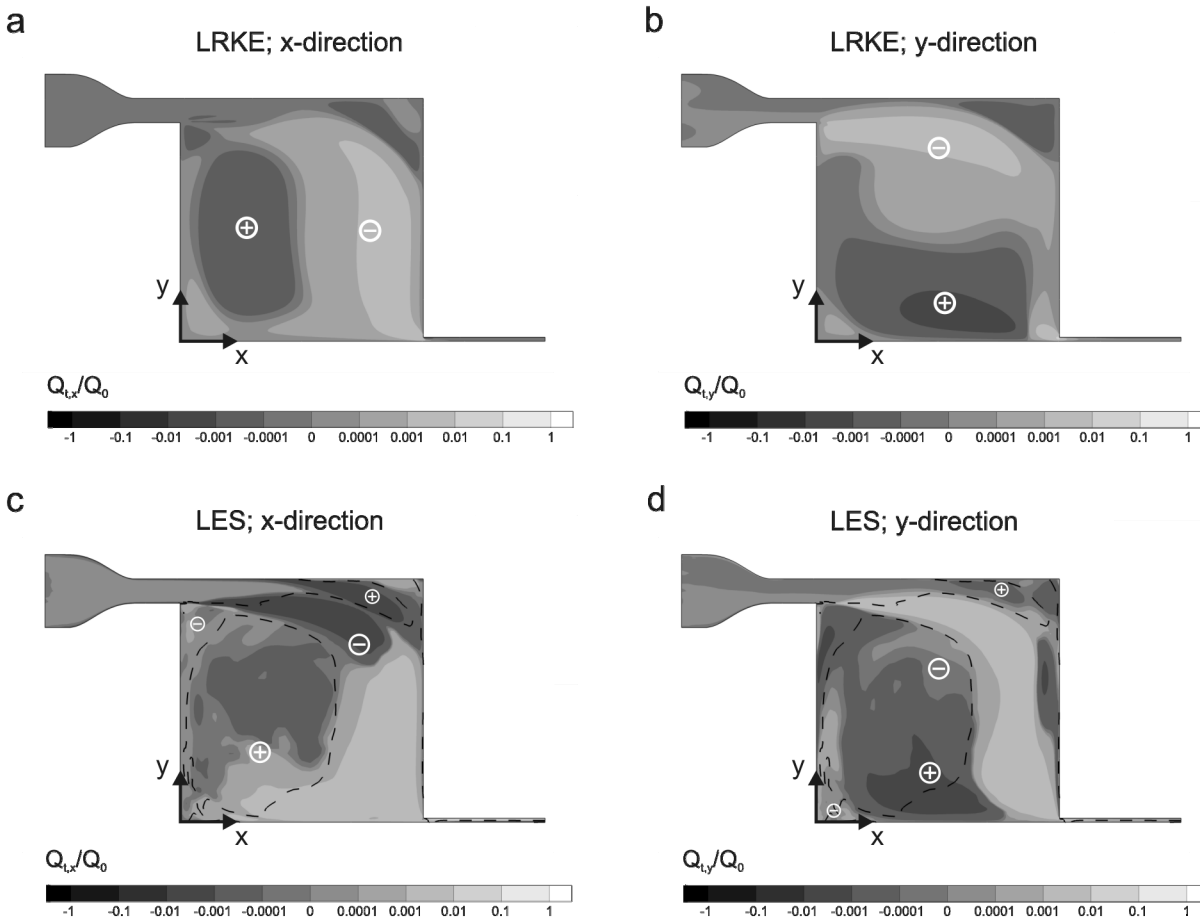

Fig. 6: Contours of the streamwise ($Q_{t,x}/Q_0$) (a,c) and vertical ($Q_{t,y}/Q_0$) (b,d) non-dimensional turbulent mass fluxes in the vertical centre plane (z/L = 0.5) of the enclosure obtained with (a,b) steady RANS and (b,d) LES. The dashed lines in (c,d) represent the isolines $\partial C/\partial x_i = 0$ in the corresponding direction: (c) $x_i = x$, (d) $x_i = y$. On each side of the isoline, the sign of $\partial C/\partial x_i$ is indicated in circles (+: positive; -: negative). The CG mechanism of turbulent mass transport is characterised by $Q_{t,i}/Q_0$ and $\partial C/\partial x_i$ having the same sign.

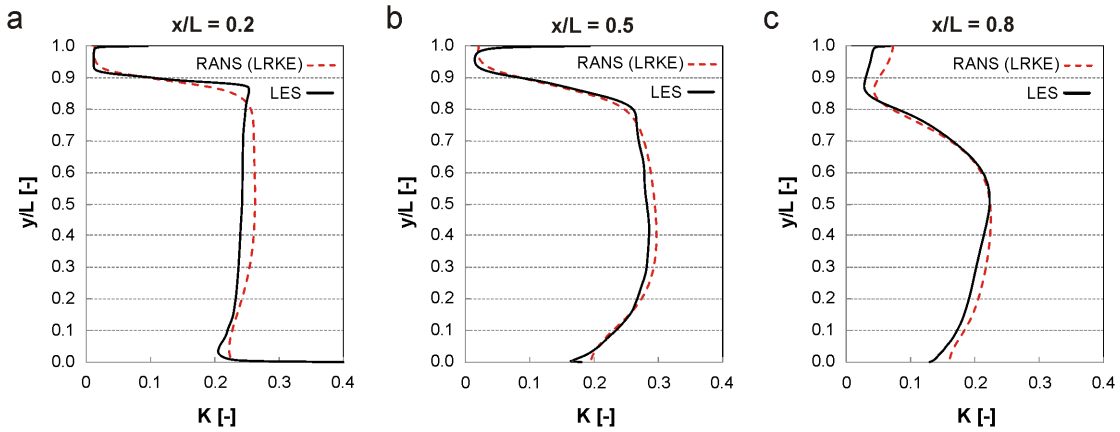

Fig. 7: Vertical profiles of dimensionless concentration K obtained with the LR k-ε model and a Sc_t value of 0.7 and with LES. (a) x/L = 0.2; (b) x/L = 0.5; (c) x/L = 0.8.

DISCUSSION

This study has presented an analysis of the validity of the standard GD hypothesis for indoor dispersion modelling. Future work will focus on additional room geometries and flow configurations, including different slot Reynolds numbers. Also, the use of different formulations for the turbulent pollutant flux in RANS simulations can be considered, such as the generalized GD hypothesis (Daly and Harlow 1970) and the high-order GD hypothesis (Abe and Suga 2001). Future work will also consist of validating both ventilation flow and pollutant concentrations in an enclosure by means of experiments.

CONCLUSIONS

This study has presented an analysis of the validity of the standard gradient-diffusion (GD) hypothesis for indoor dispersion modelling in an enclosure ventilated by a transitional wall jet (Re ≈ 2,500). This is important because the standard GD hypothesis is often applied in ventilation studies, as well as in other research areas, to model the turbulent mass flux in steady RANS simulations of pollutant dispersion. The following conclusions can be made:

- The convective mass fluxes obtained with LES and RANS are nearly identical.
- The convective mass fluxes are at least one order of magnitude larger than the turbulent fluxes, indicating the stronger importance of the transport by the mean flow in the overall dispersion process in the enclosure compared to transport by the turbulent fluctuations.
- The results of the turbulent fluxes obtained with the LES simulation have shown that counter-gradient mechanisms are present inside the enclosure. As a result, the standard GD hypothesis is not valid in the entire flow domain. However, since the convective mass fluxes dominate over the turbulent mass fluxes for this particular case, the predicted pollutant concentration in the enclosure does not differ significantly (within 10%) as a result of this deficiency.

REFERENCES

Abe, K., Suga, K., 2001 Toward the development of a Reynolds-averaged algebraic turbulent scalar flux model. International Journal of Heat and Fluid Flow, 22: 19-29.

Awbi, H.B., 2003. Ventilation of buildings. London: Spon Press.

Chang, K.C., Hsieh, W.D., Chen, C.S., 1995. A modified low-Reynolds-number turbulence model applicable to recirculating flow in pipe expansion. Journal of Fluids Engineering, 117: 417-423.

Chen, Q., 1995. Comparison of different k-ε models for indoor air-flow computations. Numerical Heat Transfer Part B: Fundamentals, 28: 353-369.

Chen, Q., 1996. Prediction of room air motion by Reynolds-stress models. Building and Environment, 31: 233-244.

Daly, B.J., Harlow, F.H., 1970. Transport equations in turbulence. Physics of Fluids, 13: 2634–2649.

Fluent Inc., 2006. Fluent 6.3 user's guide, Lebanon.

Germano, M., Piomelli, U., Moin, P., Cabot, W.H., 1991. A dynamic subgrid-scale eddy viscosity model. Physics of Fluids, A 3: 1760-1765.

Gousseau, P., Blocken, B., van Heijst, G.J.F., 2011. CFD simulation of pollutant dispersion around isolated buildings: On the role of convective and turbulent mass fluxes in the prediction accuracy. Journal of Hazardous Materials, 194: 422-434.

Gousseau, P., Blocken, B., van Heijst, G.J.F., 2012. Large-Eddy Simulation of pollutant dispersion around a cubical building: Analysis of the turbulent mass transport mechanism by unsteady concentration and velocity statistics. Environmental Pollution, 167: 47-57.

Lilly, D.K., 1992. A proposed modification of the Germano subgrid-scale closure method, Phys. Fluids A 4, 633-635.

Moin, P., Squires, K., Cabot, W., Lee, S., 1991. A dynamic subgrid-scale model for compressible turbulence and scalar transport. Physics of Fluids A3-11: 2746-2757.

Nielsen, P.V., 1974. Flow in air conditioned rooms, PhD Thesis, Technical University of Denmark, Copenhagen.

Sergent, E., 2002. Vers une méthode de couplage entre la simulation des grandes échelles et les modèles statistiques. Thèse présentée devant l'Ecole Centrale de Lyon.

Smagorinsky, J., 1963. General circulation experiments with the primitive equations. I. The basic experiment. Monthly Weather Review, 91: 99-164.

Tominaga, Y., Stathopoulos, T., 2007. Turbulent Schmidt numbers for CFD analysis with various types of flowfield. Atmospheric Environment, 41: 8091-8099.

van Hooff, T., Blocken, B., 2010. Coupled urban wind flow and indoor natural ventilation modelling on a high-resolution grid: A case study for the Amsterdam ArenA stadium. Environmental Modelling & Software, 25(1): 51-65.

van Hooff, T., Blocken, B., Defraeye, T., Carmeliet, J., van Heijst, G.J.F., 2012a. PIV measurements of a plane wall jet in a confined space at transitional slot Reynolds numbers. Experiments in Fluids, 53(2): 499-517.

van Hooff, T., Blocken, B., Defraeye, T., Carmeliet, J., van Heijst, G.J.F., 2012b. PIV measurements and analysis of transitional flow in a reduced-scale model: ventilation by a free plane jet with Coanda effect. Building and Environment, 56: 301-313.

van Hooff, T., Blocken B., van Heijst, G.J.F., 2012c. On the suitability of steady RANS CFD for forced mixing ventilation at transitional slot Reynolds numbers. Indoor Air, doi: 0.1111/ina.12010.